energies

MDPI

Article

An Integrated Approach to Reservoir Characterization for Evaluating Shale Productivity of Duvernary Shale: Insights from Multiple Linear Regression

Gang Hui [1,2,*], Fei Gu [3], Junqi Gan [3], Erfan Saber [4] and Li Liu [3]

[1] State Key Laboratory of Petroleum Resources and Prospecting, China University of Petroleum Beijing, Beijing 102249, China
[2] Department of Chemical and Petroleum Engineering, University of Calgary, Calgary, AB T2N 1N4, Canada
[3] Research Institute of Petroleum Exploration and Development, China National Petroleum Corporation, Beijing 721002, China
[4] School of Mechanical and Mining Engineering, The University of Queensland, Saint Lucia, QLD 4072, Australia
* Correspondence: hui.gang@cup.edu.cn

Abstract: In the development of unconventional shale resources, production forecasts are fraught with uncertainty, especially in the absence of a full, multi-data study of reservoir characterization. To forecast Duvernay shale gas production in the vicinity of Fox Creek, Alberta, the multi-scale experimental findings are thoroughly evaluated. The relationship between shale gas production and reservoir parameters is assessed using multiple linear regression (MLR). Three hundred and five core samples from fifteen wells were later examined using the MLR technique to discover the fundamental controlling characteristics of shale potential. Quartz, clay, and calcite were found to comprise the bulk of the Duvernay shale. The average values for the effective porosity and permeability were 3.96% and 137.2 nD, respectively, whereas the average amount of total organic carbon (TOC) was 3.86%. The examined Duvernay shale was predominantly deposited in a gas-generating timeframe. As input parameters, the MLR method calculated the components governing shale productivity, including the production index (PI), gas saturation (S_g), clay content (V_{cl}), effective porosity (F), total organic carbon (TOC), brittleness index (BI), and brittle mineral content (BMC) (BMC). Shale gas output was accurately predicted using the MLR-based prediction model. This research may be extended to other shale reservoirs to aid in the selection of optimal well sites, resulting in the effective development of shale resources.

Keywords: unconventional shale productivity; mineralogy; petrophysics; geochemistry; geomechanics; multiple linear regression

Citation: Hui, G.; Gu, F.; Gan, J.; Saber, E.; Liu, L. An Integrated Approach to Reservoir Characterization for Evaluating Shale Productivity of Duvernary Shale: Insights from Multiple Linear Regression. *Energies* **2023**, *16*, 1639. https://doi.org/10.3390/en16041639

Academic Editor: Reza Rezaee

Received: 22 November 2022
Revised: 14 January 2023
Accepted: 2 February 2023
Published: 7 February 2023

1. Introduction

With the success of the shale gas revolution in the United States, the competition and trade pattern of the global natural gas market have undergone significant changes in recent years. This has had a significant impact on the global oil and gas supply pattern, as well as geopolitics [1–3]. According to worldwide production data, shale gas production reached 7688 $\times$ 10^8 m^3 by the end of 2020, accounting for 19.6% of the total natural gas output (i.e., 39,180 $\times$ 10^8 m^3) [4]. The shift from conventional to unconventional resources was accomplished with the development of shale resources [3]. Canada is the second nation, after the United States, to effectively explore and extract shale gas as an essential component of the North American unconventional energy sector [5]. Canada's shale gas output reached 58 $\times$ 10^8 m^3 by the end of 2021, ranking it fourth in the world after the United States (7572 $\times$ 10^8 m^3), China (228 $\times$ 10^8 m^3), and Argentina (128 $\times$ 10^8 m^3). Among basins containing shale gas, the Duvernay shale basin plays a major role in shale gas

production [6,7]. In recent decades, the widespread use of multistage hydraulic fracturing technology [8] has transformed the Duvernay shale deposit into a world-class unconventional resource play.

Numerous studies on the development of shale gas in North America have been undertaken, covering the major technologies of shale gas production [9,10], shale gas resource appraisal [11,12], and the governing factors of shale gas sweet spots [13]. In addition, several studies have been conducted to anticipate shale production. Several geological factors, including preservation conditions (e.g., burial depth, temperature, pressure, and sedimentary thickness of shale), organic matter quality (e.g., the type, content, and maturity of organic matter), mineral quality (e.g., the content of brittle minerals and clay), petrophysical features (e.g., porosity, permeability, free gas, and adsorbed gas content), and organic matter quality (e.g., the and type and content [1,14,15]). In addition to the aforementioned geological factors, operational factors (e.g., the shale brittleness index (BI), derived from Poisson's ratio and Young's modulus) and operational parameters (e.g., number of fracturing stages, horizontal length, fracturing fluid injection volume, and proppant placed mass for horizontal wells) have also had a significant impact on shale gas production [14,16–18]. Some researchers have also presented a system that combines thin-section observations, three-dimensional (3D) seismic data, and picture logs to assess reservoir parameters and anticipate probable development sites [19]. Consequently, it is essential to measure the effects of these geological and operational factors on shale gas resource development.

However, there are few feasible scenarios for the development of a single shale reservoir based on a complete, multi-data analysis, especially the integration of mining, geochemistry, petrophysics, and geomechanics assessments. In addition, a comprehensive data analysis is often conducted to establish the criteria for the magnitude range of the selected regulatory components that contribute to the shale sweet spot. The sweet spot zone is then predicted based on these criteria [18,20]. However, the subjectivity (e.g., researcher bias) and unpredictability of the selection of elements governing shale output reduce the accuracy of the sweet spot zone projection. Nonetheless, as a method of mass -information data mining, machine learning algorithms (e.g., regression algorithm, neural network method, decision learning, and the Bayesian method) can identify the controlling factors that contribute the most to shale sweet spot prediction by detecting the hidden relationships between various controlling factors. The use of machine learning in oilfield development, based on massive geological and operational data, has revealed a variety of potential growth benefits [11,17,21,22]. Some researchers provided a deep learning technique (e.g., the construction of a deep-feed neuro-network model) for predicting shear velocity from traditional logging curves in a confined sandstone reservoir [23]. Other researchers proposed an integrated method of petro-physical, mineral composition, well-log facies, and horizon attribute analyses, as well as an unsupervised vector quantizer artificial neural network (UVQ-ANN) and sequential indicator simulation (SIS) modeling, which was used to evaluate the prospect of a gas reservoir [24].

However, production forecasts for the exploitation of unconventional shale resources are fraught with uncertainty, especially in the absence of a full, multi-data analysis of reservoir characterization. In this work, an integrated reservoir characterization method was suggested in order to assess the shale productivity of Duvernay shale. Mineralogy, geochemistry, petrophysics, and geomechanics evaluations were included in the entire reservoir characterization. Multiple linear regression (MLR) was used to quantify the relationship between shale productivity and reservoir features and to determine the most influential components that contribute to shale productivity. Finally, a prediction model of shale productivity was created, providing the groundwork for the future efficient development of shale gas resources in this region.

2. Field Background

The Western Canadian Sedimentary Basin (WCSB) deposited the Duvernay Formation during the Upper Devonian period (Figure 1a) [25,26]. In addition, the Duvernay Formation

is a significant source of oil and gas for the Leduc and Swan Hills reservoirs (Figure 1b,d). The Grosmont carbonate platform divides the Duvernay shale into two sections: the Western Shale Basin (WSB) and the Eastern Shale Basin (ESB) (ESB). Rokosh et al. (2012) calculated the sediment thickness and contoured the net shale thickness distribution by setting the gamma line cutoff to 105 API (Figure 1c) [7]. Resources are abundant in the Duvernay shale, and the production of oil and gas is enormous. The overall area of the Duvernay shale is roughly 2.43×10^4 km^2, and its natural gas, liquid hydrocarbon, and crude oil reserves are 23.22×10^{12} m^3, 115.54×10^8 t, and 250.5×10^8 t, respectively [27,28].

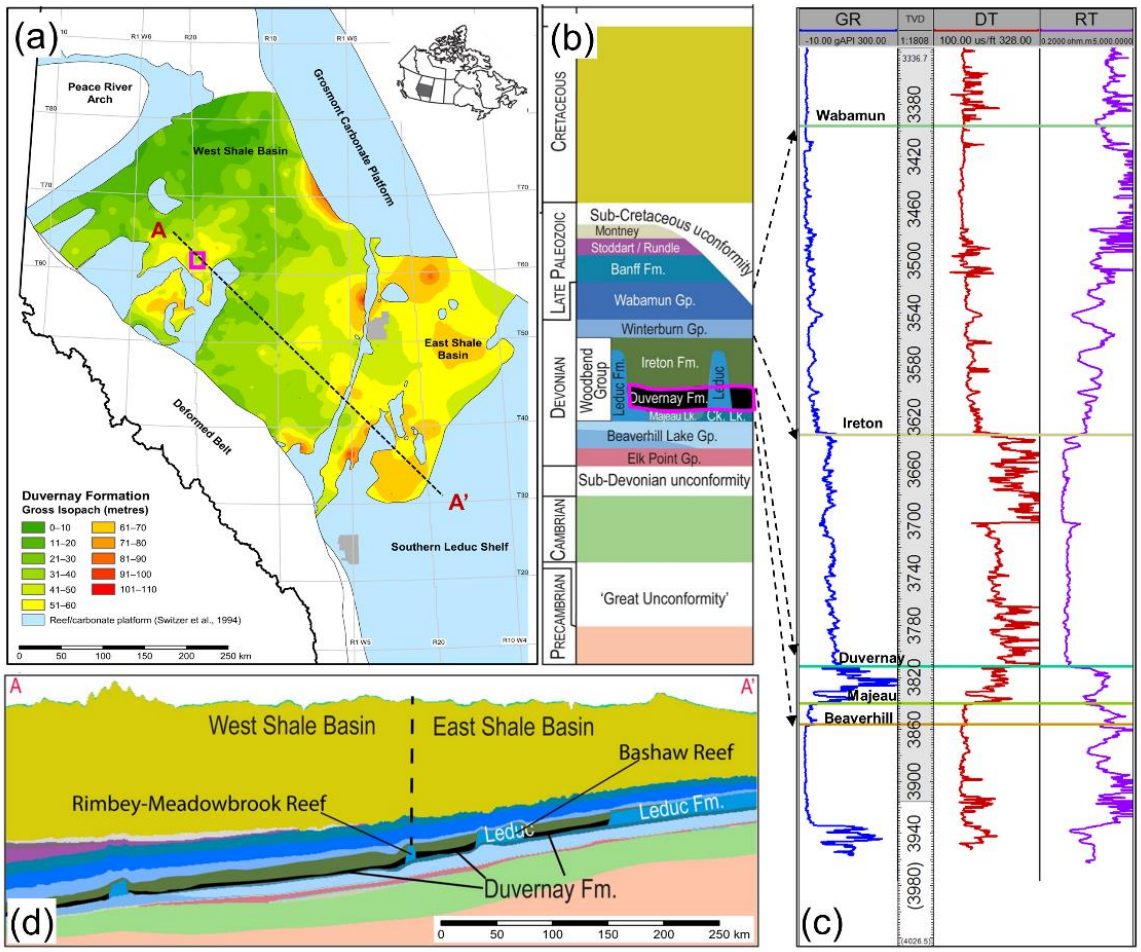

Figure 1. The geological information of the Duvernay formation. (**a**) Location of the West Shale Basin (WSB) and East Shale Basin (ESB). The examined region is marked by the small magenta box. (**b**) Stratigraphy of the studied region. The magenta polygon marks the Duvernay formation with the black shale lithology. (**c**) The logging response of associated formations. GR—Gamma ray; DT—Acoustic sonic; and RT—Formation resistivity. (**d**) The cross-sectional stratigraphy for lines A-A′ in (**a**).

The kerogen of the Duvernay shale has been classified as type II, with total organic carbon (TOC) and VR values ranging from 0.1 to 11.1 and 0 to 2.0 (wt%), respectively. In addition, from the northeast to the southwest, the age of the organic matter (i.e., kerogen) increases gradually. The upper Duvernay Formation is typically located between 1000 and 5500 m below the surface. According to previous evaluations, the Duvernay Formation in the Kaybob region is the most commercially significant shale formation in the WCSB [5,7,22]. Throughout the logging reaction, the Duvernay shale exhibits low gamma ray, moderate acoustic log, and high formation resistivity (Figure 1c) [29].

The Kaybob part of the western shale basin contains the Duvernay shale, also known as the Fox Creek shale, which is located close to the Fox Creek region (Figure 1a). This study collected data on geology, completion, logging, testing, and fracturing treatments

using the Geoscout database (https://www.geologic.com/products/geoscout accessed on 1 November 2022). One hundred and thirty horizontal wells were drilled and hydraulically fractured in the Duvernay formation (Figure 2). Experiments including mineralogy, geophysics, and geochemistry, and geomechanics made use of core samples from thirteen coring wells (Figure 2). A typical horizontal well had 39 fracturing phases and a horizontal section that measured 2127 m. Moreover, the average volumes of proppant deposited and fluid pumped were 5650 tons and 39,273 m^3, respectively. The average fracture depth was 3317 m beneath the surface. As a consequence of fracturing stimulation, the initial one-year shale gas production equivalent per stage ranges from 2.6 to 48 MMcf (i.e., the total of dry gas plus condensate gas), with an average of 19.9 MMcf (Figure 2).

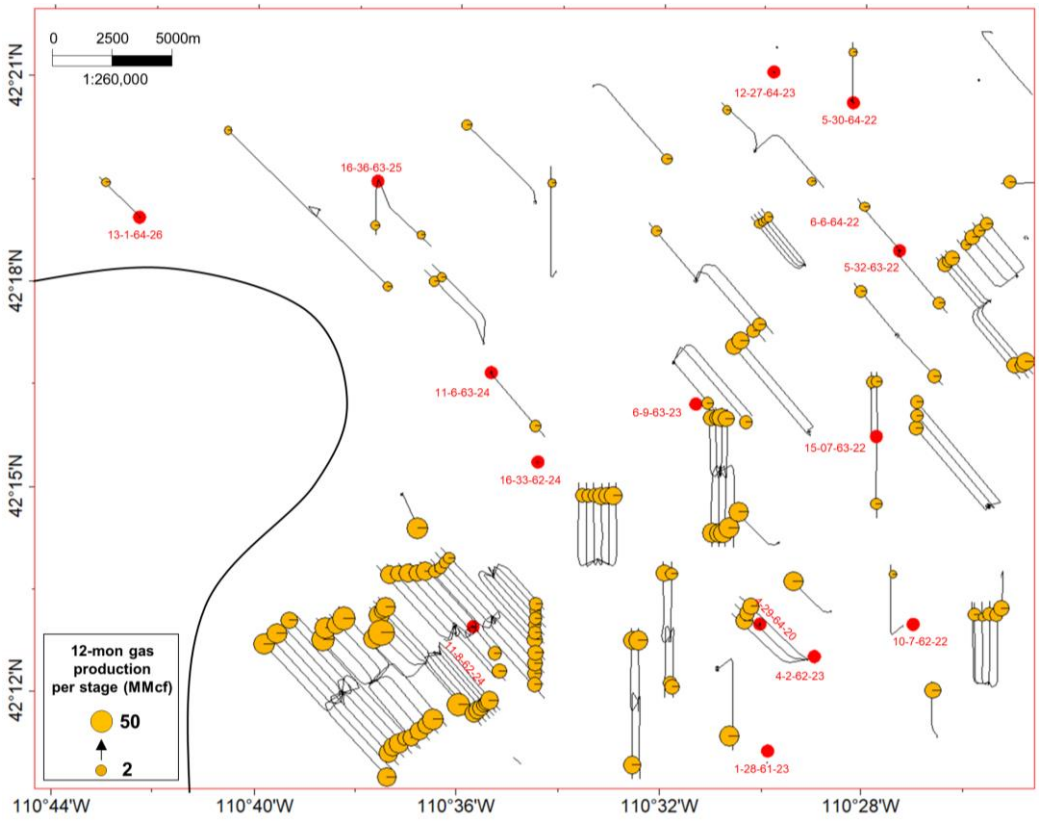

Figure 2. Locations of fractured horizontal wells and coring wells. The black line denotes the trajectory of horizontal wells. Coring wells are labeled with red color. The yellow circle represents the magnitude of the one-year gas production equivalence per stage for horizontal wells, scaled by production magnitude. The left black curve denotes the boundary line of the Duvernay formation.

3. Methodology

In this work, an integrated reservoir characterization technique was presented to estimate the productivity of Duvernay shale. Integrated assessments of mineralogy, geochemistry, petrophysics and geomechanics were used to undertake a full reservoir characterization. Using X-ray diffraction mineralogy measurements, the lithology characteristics of the shale were determined. The storage and flowability of the shale were determined using a tight rock analysis. The geochemical parameters of Rock-Eval Pyrolysis described the quality of organic materials. The rock's compressibility was determined by uniaxial and triaxial compression. MLR was used to quantify the relationship between shale productivity and reservoir features and to determine the most influential components contributing to shale productivity. Finally, a model of shale productivity prediction was built. Figure 3 depicts the process flow.

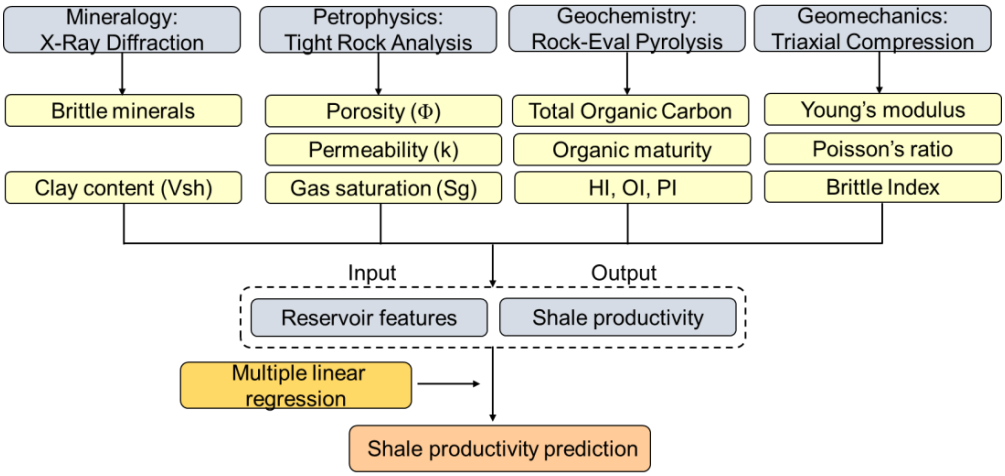

Figure 3. Sketch diagram of shale productivity evaluation in unconventional shale reservoirs.

3.1. Experimentally Based Reservoir Parameters

Mineralogy experiments. The X-ray diffraction process experiments were carried out using a thin section apparatus and a field emission scanning electron microscope (FESEM). The mineralogy of core materials was then identified using peak-profile and whole-pattern fitting techniques. Finally, a semi-quantitative evaluation of the whole rock was performed to determine the overall mineralogy and clay content (V_{cl}) of the bulk samples [22].

Petrophysics experiments. The effective porosity and grain density of crushed samples were evaluated, and the bulk density of entire samples was determined. Interstitial water was collected after the samples were weighed, placed in a retort, heated to the temperature of formation, and cooled. The bulk and grain density, effective porosity (Φ), and gas saturation (S_g) were eventually estimated based on pre- and post-retorting measurements [30].

Geochemistry investigations. For analyzing rock samples, a Rock-Eval instrument was required. A sample was pyrolyzed at a predetermined temperature under nitrogen, the produced hydrocarbons were identified, and CO and CO_2 were continually detected by the infrared detectors. The sample was then oxidized in air at the desired temperature while infrared detectors continuously measured CO and CO_2. Geochemical parameters were derived from this data [11,31].

Geomechanics experiments. Uniaxial and triaxial compression tests were performed. Under conditions of unlimited compression, the maximal compressive strength of the core samples was determined. On vertical, 45 degree, and horizontal samples, triaxial compression tests were performed in combination with ultrasonic velocity data. To calculate the applied stress, it was necessary to measure the applied pressure and load with a calibrated pressure gauge. The static Young's modulus and Poisson's ratio were then immediately calculated during each test [32]. Using these two variables, the brittleness index was computed [33–35].

After collecting these four types of core measurements from coring wells, the average value of such a measurement was derived to indicate the distinct reservoir characteristic of each coring well. The distribution of these reservoir properties was then calculated using the sequential Gaussian stochastic (SGS) model. The SGS method is a stochastic interpolation approach based on the Kriging algorithm that may be used to produce maps containing information on sites (i.e., wells) with a certain reservoir feature. The technique for its computation is thoroughly detailed in our prior paper [36].

3.2. Multiple LINEAR Regression Approach

Given that various linked parameters have separate units, it is necessary to execute data standardization to reduce the units' disparities. For factors that are positively connected to gas production, the following equation is employed for data standardization:

$$x_i = \frac{a_i - a_{min}}{a_{max} - a_{min}} \tag{1}$$

where x_i is the ith standardized independent variable; a_i is an original independent variable at one site; and a_{max} and a_{min} are the maximum and minimum value among all "a" values, respectively.

Moreover, for parameters that are negatively related to gas production, the equation of data standardization is shown as:

$$x_i = \frac{a_{max} - a_i}{a_{max} - a_{min}} \tag{2}$$

MLR is a statistical approach that forecasts the distribution of a dependent variable using a number of independent factors [37]. The objective of the MLR method is to establish the linear connection between the independent and dependent characteristics that impact a given event. MLR is an extension of classic least-squares regression since it employs multiple explanatory factors.

$$y = \beta_0 + \beta_1 x_1 + \cdots \beta_i x_i + \cdots + \beta_n x_n + \varepsilon, \tag{3}$$

where y is the dependent variable; $x_1 \ldots x_n$ are independent variables; β_0 is the y-intercept; β_i is the regression coefficient of the ith independent variables; ε is the model error, also known as the residuals.

The determination coefficient (R^2) and magnitude of a squared error (MSE) can be used to evaluate the prediction performance of the MLR-based model by

$$\text{MSE} = \frac{\sum_{j=1}^{n} (y_j - \hat{y}_j)^2}{n}, \tag{4}$$

$$R^2 = 1 - \frac{\sum_{j=1}^{n} (y_j - \hat{y}_J)^2}{\sum_{j=1}^{n} (y_j - \overline{y_j})^2}, \tag{5}$$

where y_j is the jth parameter after normalization; $\hat{y}_j$ is the predicted jth parameter; $\overline{y_j}$ is the mean value of predicted parameters; and n is the number of parameters.

Reservoir characteristics derived from core experiments, such as the mineral contents and shale content (mineralogy), porosity, permeability, and gas saturation (petrophysics), total organic carbon and production index (PI) (geochemistry), and the brittleness index derived from Young's modulus and Poisson's ratio (mechanical properties), were the input variables for this study (geomechanics). In addition, the output variable contains the initial one-year equivalent gas production per stage [21]. Using MLR, the relationship between the shale productivity and the reservoir parameters was quantified further.

4. Results

4.1. Characterization of Reservoir Properties

4.1.1. Mineralogy Characterization

The thin section findings of two typical cores are shown in Figure 4a,b. Figure 4a depicts a quartzose siltstone that is fairly laminated and abundant in fossils and pyritic and argillaceous material. Feldspars, silt-sized detrital quartz grains, and abundantly comminuted bioclasts are also reported to exist within a densely packed, silty, clay-rich matrix. It was also discovered that dolomites, pyrite, and marcasite partially replace fossils and matrices. Sub-horizontal discontinuous laminae are represented by biological waste,

micas, clay minerals, and detrital silt. The fact that bitumen fills interparticle micropores was also established, as measured by FESEM. Overall, the thin section includes 43% silt, 24% clay, and 24% carbonate, in that order.

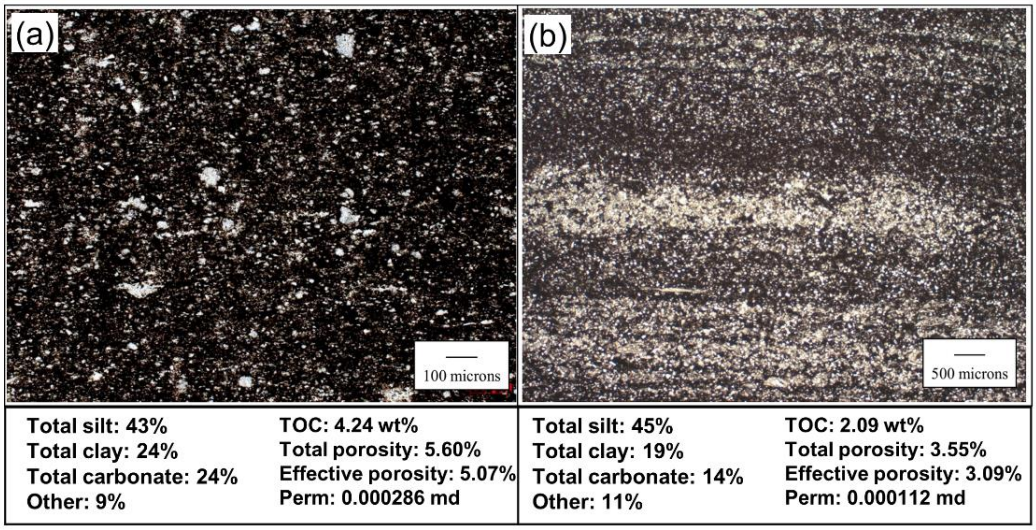

Figure 4. (**a**,**b**) Mineralogy features of two representative thin sections.

The interlaminated siltstone and silty mudstone shown in the small slice of Figure 4b is another example. Large numbers of silt-sized detrital quartz and feldspar grains produce siltstone laminae that are densely packed and cemented with calcite. In addition, mudstone laminae, alternating pyrite, calcite, and Fe-dolomite/ankerite with a dense, clay- and organic-matter-rich matrix are exhibited. Notable characteristics include the organization of organic waste, micas, dolomite, and silt in discontinuous, sub-horizontal laminae. The photograph with the higher magnification appears to be illuminated by polarized light that has been reversed. The final mineralogy measurements for this thin section are as follows: 45% silt, 19% clay, and 14% carbonate.

X-ray diffraction measurements of core samples from thirteen coring wells were collected, and the results are depicted in Figure 5 [29]. Quartz ranged from 32.4% to 50.9% (43.2% on average) in the Duvernay shale of the investigated region, whereas clay ranged from 14.2% to 34.5% (23.6% on average) and calcite ranged from 5.2% to 39.3% (14.3% on average). As brittle minerals include quartz, feldspar, and calcite, we would estimate the brittle mineral content (BMC) by analyzing the concentrations of these three minerals in the region under investigation.

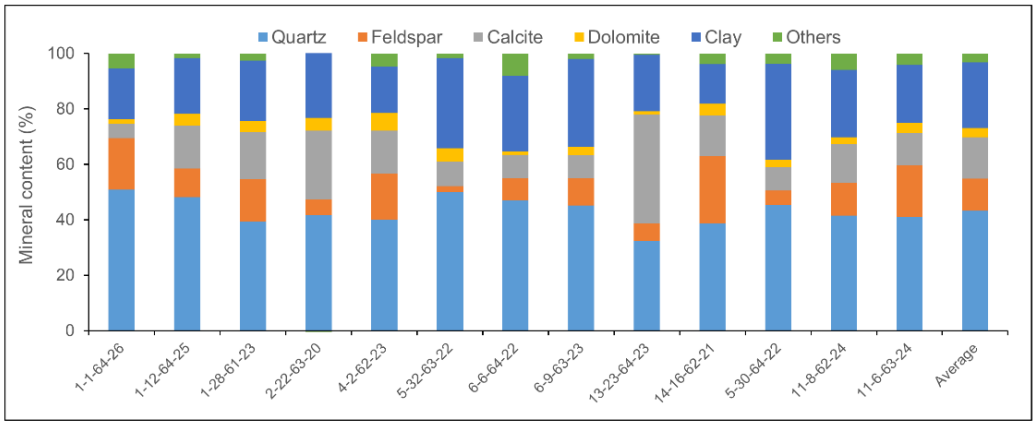

Figure 5. Mineralogy measurements for coring wells. Clay, quartz, feldspar, and calcite are primary minerals.

Utilizing the SGS technique outlined in Section 3.1, the spatial characteristics of brittle minerals and clay minerals were determined. The correlation's one-year gas production equivalency is depicted in Figure 6a,b. In contrast to clay minerals, brittle minerals have a distinct distribution pattern. In the northeast sector of the investigated region, brittle minerals have low values that correlate to low one-year gas production equivalences, whereas the other region has comparatively high values and high gas production equivalences. As a result of the clay material's opposing geographical properties, a high value is seen towards the northeast. As one of the input variables, information on mineralogy will be utilized to discover the parameters that affect shale productivity.

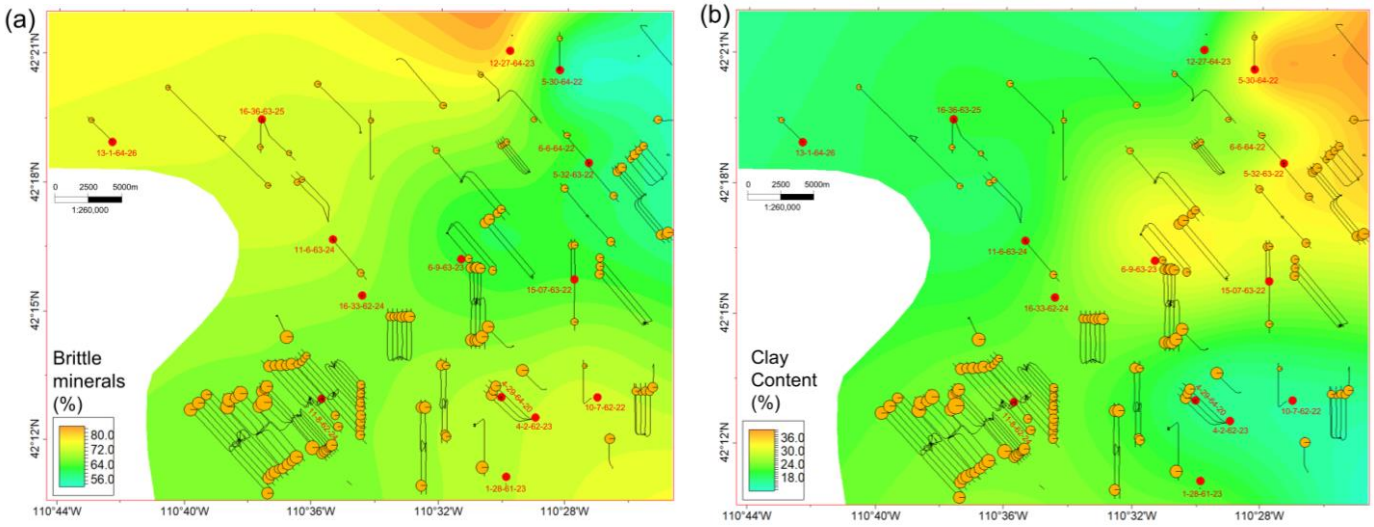

Figure 6. Map view of (**a**) brittle minerals (%) (i.e., quartz plus feldspar and calcite minerals) and (**b**) clay content (%). The grey circle represents the 1-year gas production equivalence per stage for horizontal wells, scaled by production values.

4.1.2. Petrophysics Characterization

The FESEM observation first established the pore type of the Duvernay shale in the study region. It is known that the Duvernay shale contains five basic types of pore structure, including the organic pore, the intergranular pore, the intragranular pore, the dissolved pore, and the grain edge pore [22]. Figure 7a illustrates the organic pore that encompasses the organic material. The organic material reveals minute fractures. In the northeast section of Figure 7b, the intergranular and intragranular pores of clay aggregates were illustrated. In addition, Figure 7c depicts a series of holes that have been dissolved in calcite rocks. The disintegration of these holes reveals the existence of organic substances. Figure 7d depicts the grain edge pore near quartz crystals.

The findings of the petrophysical measurements of the tight rock analysis for 11 coring wells are displayed in Figure 8 [29]. The effective porosity of the shale ranged from 1.55 to 6.12 percent, with a typical value of 3.96 percent. The core's permeability varied from 0.26 nD to 335.6 nD, with a mean of 137.2 nD. The measured range of gas saturation was between 28.98% and 78.6%, with an average of 59.74%.

In Figure 9a,b, the SGS approach was utilized to illustrate the spatial characteristics of petrophysical parameters. It is demonstrated that the northern and eastern portions of the region have low porosity and gas saturation, which is compatible with the area's poor one-year gas equivalent production. It is feasible that the region with the highest porosity and gas saturation will have the highest gas output equivalent. Similarly, petrophysical data is used as one of the input factors to discover the variables that impact shale productivity.

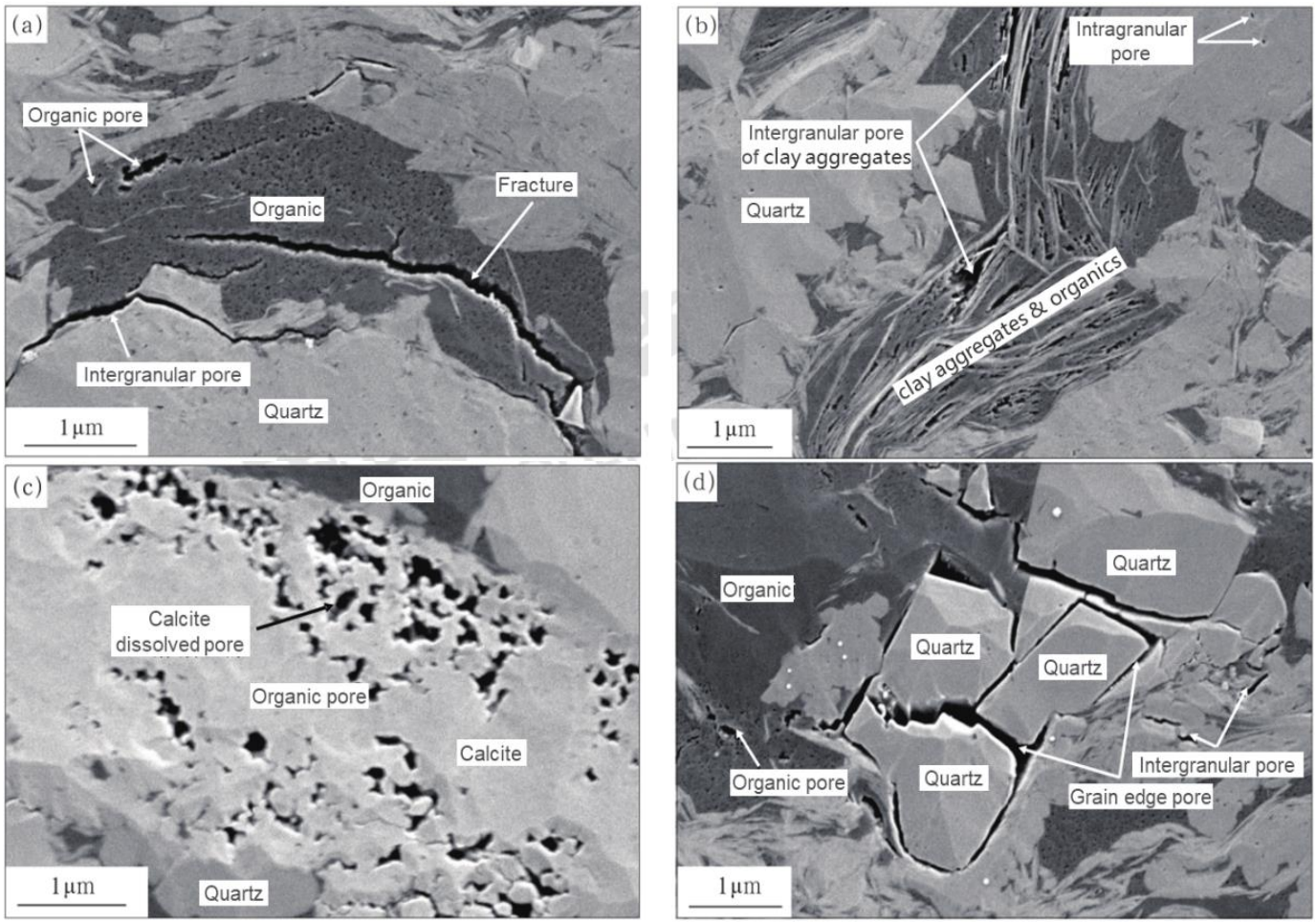

Figure 7. Primary pore type for the Duvernay shale in the examined region: (**a**) organic pore and intergranular pore, (**b**) intergranular pore and intragranular pore, (**c**) dissolved pore and organic pore, and (**d**) grain edge pore, organic pore, and intergranular pore.

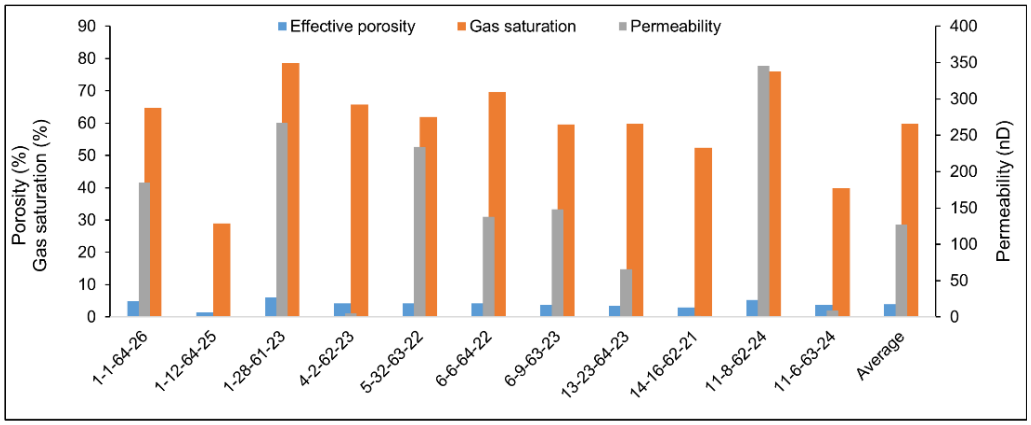

Figure 8. Petrophysical measurements of effective porosity, permeability, and gas saturation for coring wells.

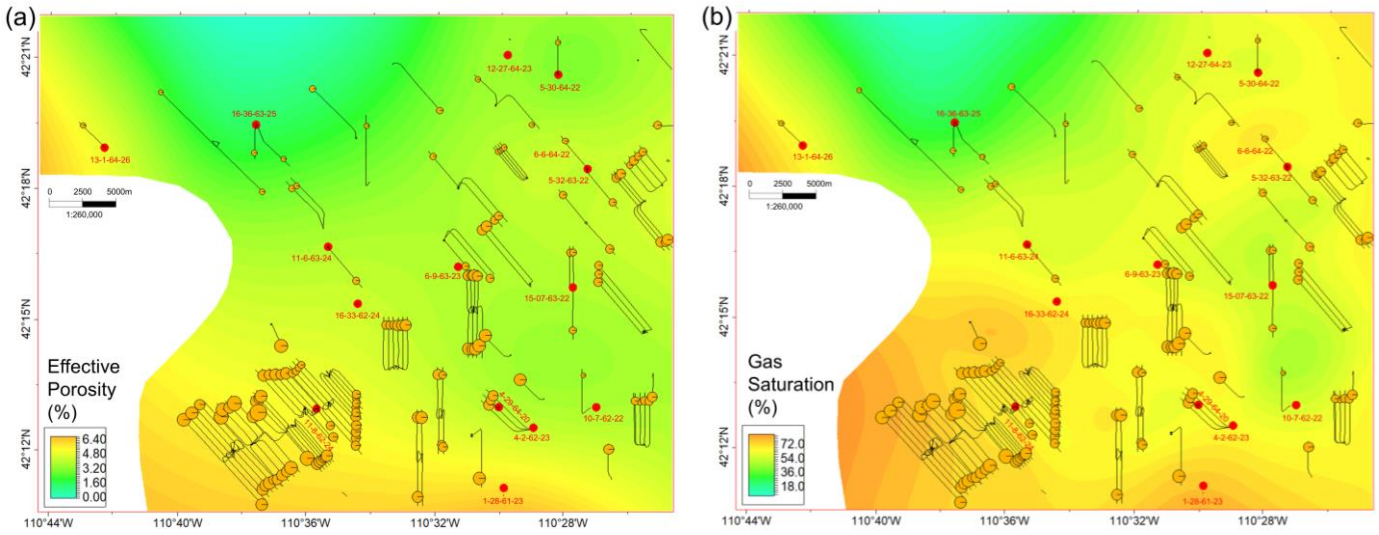

Figure 9. Map view of (**a**) effective porosity (%) and (**b**) gas saturation (%) in the studied region. The grey circle represents the one-year gas production equivalence per stage for horizontal wells, scaled by production values.

4.1.3. Geochemistry Characterization

Eleven Rock-Eval Pyrolysis tests from coring wells were employed to collect the geochemical results. The range of total organic carbon (TOC) was 2.32 to 5.0%, with a mean of 3.86%. The maximum pyrolysis yield temperature (T_{max}), free and adsorbed hydrocarbons (S1), and kerogen pyrolysis (S2) varied from 0.05 to 4.23 mg/g, 1.89 to 9.94 mg/g, and 449 to 482 °C, respectively. The relative ranges of the hydrogen index (HI), the oxygen index (OI), and the production index (PI) were 48.2–198.7, 0.76–16.04, and 0.02–0.64, respectively. The bulk of Duvernay shale belongs to the Type III gas-prone type and is located in the condensate-wet gas & dry gas zone, based on relationships between the geochemical features of coring wells (Figure 10a,b). The one-year shale gas equivalent, which comprises dry gas and condensate gas, is therefore assigned to our target shale production variable.

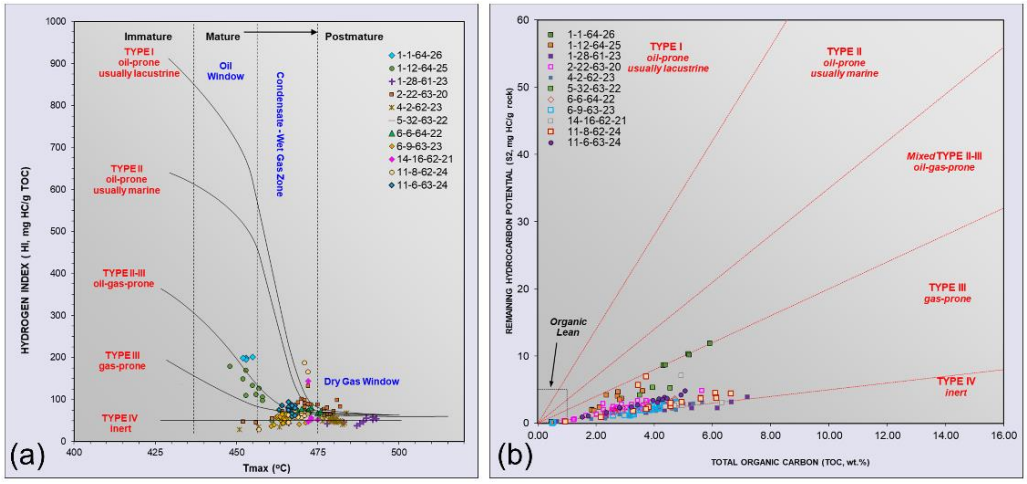

Figure 10. Geochemistry features of coring wells [38]. (**a**) Relationships between the Tmax and Hydrogen Index. (**b**) Relationship between TOC and S2.

It was demonstrated that the Duvernay shale was created predominantly in an oxygen-free saltwater environment. In addition, such shale fell inside the window for gas generation since the vitrinite reflectance varied between 1.8% and 4.1%. The SGS method was used

to extract spatial geochemical characteristics from the research region. The findings are depicted in Figure 11a,b. It can be observed that the northern region has low TOC and PI values, which are suggestive of a poor equivalent o-year gas production. Other regions of the analyzed area demonstrate high outputs, which are accompanied by elevated TOC and PI levels.

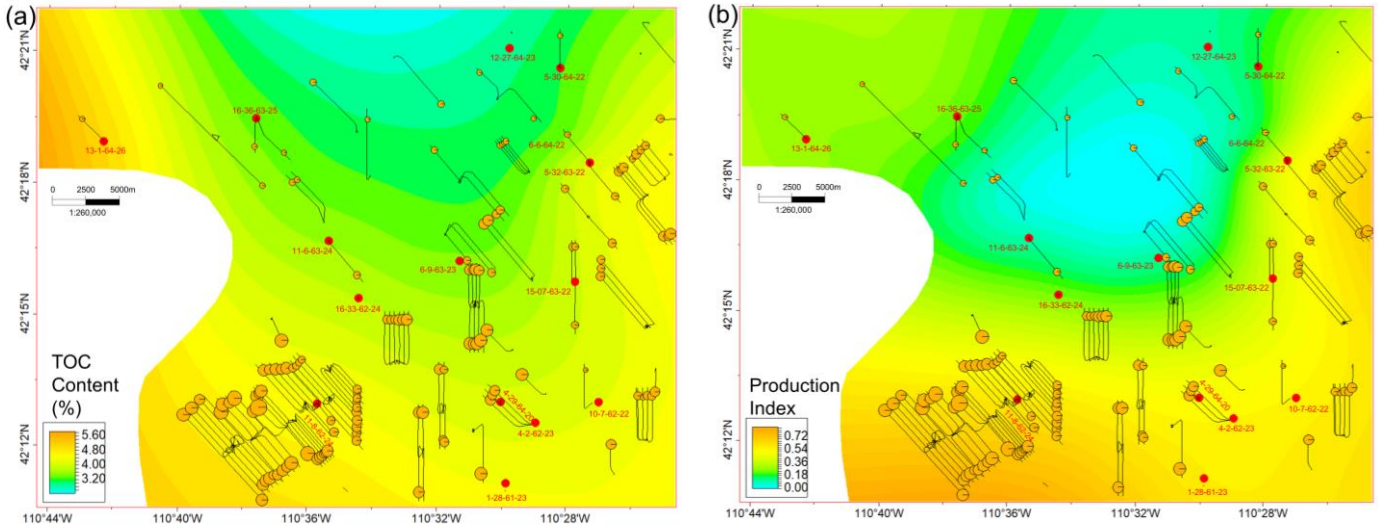

Figure 11. Geochemistry features in the examined region. (**a**) Map view of total organic carbon (TOC, wt%). (**b**) Map view of Production Index (PI). The grey circle represents the one-year gas production equivalence per stage for horizontal wells, scaled by production values.

4.1.4. Geomechanics Characterization

The measurements of triaxial compression tests for coring wells are shown in Figure 12 [33]. It was established that the axial strain and radial strain deviatory stresses varied for distinct core samples. As a result, these core samples' identified rock mechanical characteristics are equally unique. Table 1 shows a statistical breakdown of the vertically interpreted geomechanical data [29,30]. The static Young's modulus was demonstrated to have an average value of 25.68 GPa and a range of 19.51–41.26 GPa. The average static Poisson's ratio was 0.21, with a range of 0.17 to 0.25.

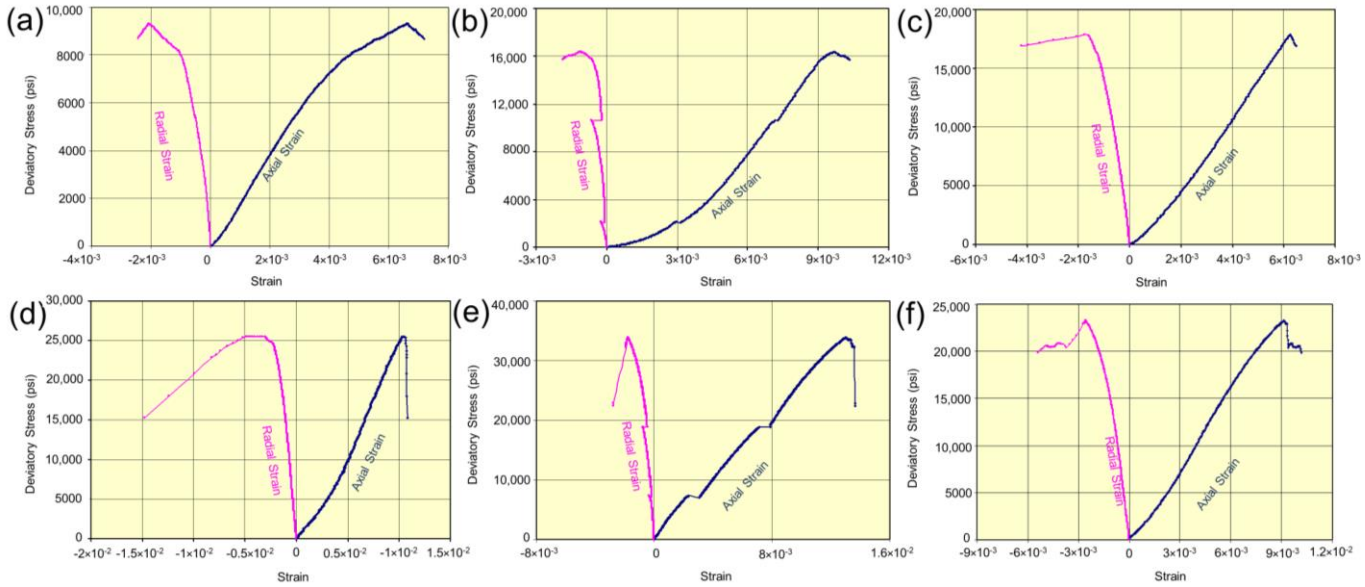

Figure 12. Measurements of the triaxial compression tests for coring wells. (**a**–**c**) Measurements for well 4-2-62-23. (**d**–**f**) Measurements for well 16-33-62-24.

Table 1. Statistics of the geomechanical measurements with vertical direction for coring wells.

Well Name	Sample Number	Depth (m)	Static Young's Modulus (GPa)	Static Poisson's Ratio	Brittleness Index
4-2-62-23	5	3615.28	21.20	0.23	0.41
	11	3632.94	22.60	0.23	0.45
	14	3639.62	21.90	0.23	0.43
4-29-64-20	FD1	3315.32	29.79	0.24	0.67
	FD2	3326.36	24.29	0.23	0.48
16-36-63-25	FD1	3548.93	24.44	0.22	0.43
	FD2	3550.4	22.74	0.21	0.32
13-1-64-26	361-8	3664.42	34.16	0.19	0.46
	361-10	3671.3	24.51	0.18	0.18
	361-5	3675.85	28.31	0.17	0.20
	361-2	3681.66	41.26	0.19	0.63
12-27-64-23	1FD	3338.92	24.32	0.18	0.17
	2FD	3343.97	25.75	0.2	0.33
16-33-62-24	6	3549.69	23.79	0.25	0.60
	FD1	3555.73	19.51	0.19	0.13
	FD2	3576.1	22.38	0.25	0.57

The Duvernay shale's brittleness was then assessed using the brittleness index (BI), which is based on both values [39,40]. The BI value for the sixteen core samples in Table 1 ranges from 0.13 to 0.67, with a mean of 0.40. Figure 13 illustrates the regional distribution of the BI according to the SGS method. The southern area has a high BI value, which indicates a substantial annual gas production. As a result, the BI value influences gas output in a beneficial manner.

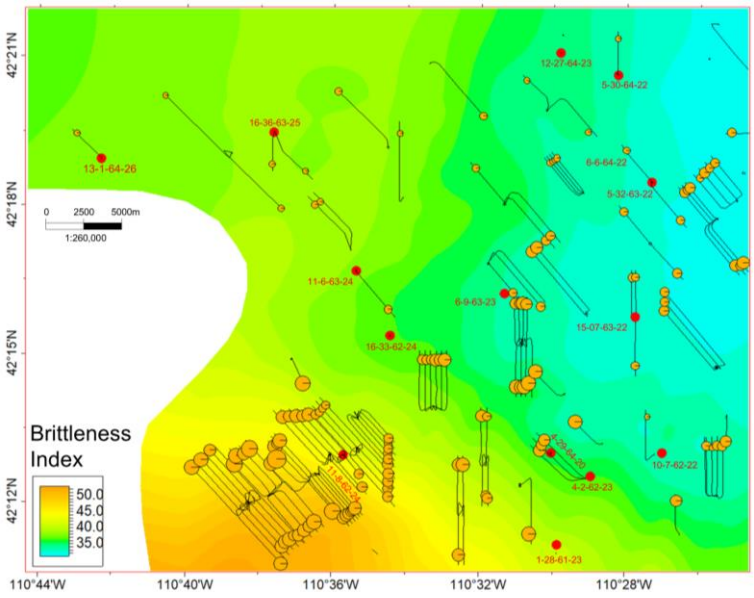

Figure 13. Map view of the brittleness index in the examined region. The grey circle represents the one-year gas production equivalence per stage for horizontal wells, scaled by production values.

4.2. MLR-Based Prediction Model

According to the geographical correlations between the one-year gas production equivalence and the seven corresponding reservoir variables, the brittle mineral content, porosity, gas saturation, total organic carbon, production index, and brittleness index are six types of features with positive associations. Only the clay content had a negative correlation with the creation of comparable gas. Equation (1) was applied to six positive

traits in order to normalize the data, whereas Equation (2) was used with the negative features. The MLR data-mining algorithm was then executed using Equation (3) through Equation (5). Finally, the outcomes of data mining for shale productivity using MLR were obtained. The weight coefficients of each input variable were computed, and the results are reported in Table 2.

Table 2. The MLR results for shale gas production equivalence in the studied region.

Type	Variables		Weight Coefficient	Rank
Input	Mineralogy	Brittle mineral content (BMC)	0.073	7
		Clay content (V_{cl})	0.161	3
	Petrophysics	Porosity (Φ)	0.136	4
		Gas saturation (S_g)	0.188	2
	Geochemistry	Total Organic Carbon (TOC)	0.115	5
		Production index (PI)	0.229	1
	Geomechanics	Brittleness index (BI)	0.098	6
Output	one-year gas production equivalence			

It is notable that the PI, Sg, Vcl, F, TOC, BI, and BMC input parameters are listed in descending order. Shale geochemistry, petrophysics, mineralogy, and geomechanics are, therefore, essential for shale production. Using these input characteristics, a prediction model of the one-year shale gas output per stage was developed using an MLR-based technique. Figure 14 depicts the distribution of predicted shale output equivalents. It can be demonstrated that the predicted shale gas production per stage during the following 12 months closely matches the actual production in this region, confirming the accuracy of our prediction model. This strategy can guide the future selection of horizontal well drilling locations and result in the efficient and cost-effective exploitation of shale resources.

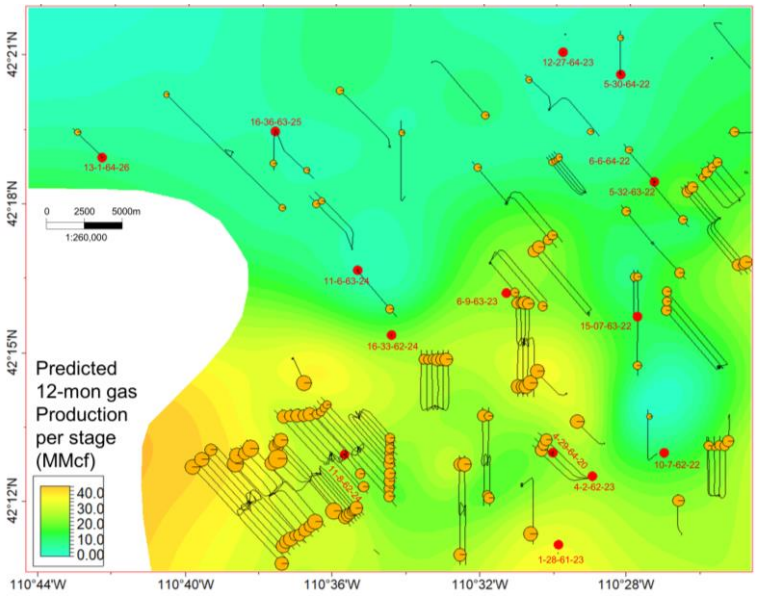

Figure 14. Prediction map of 12 mon gas production equivalence per stage via MLR approach in the studied region. The grey circle represents the actual one-year gas production equivalence per stage for horizontal wells, scaled by production values.

5. Discussions

5.1. Data Quality

The core experiment data served as the primary input for the MLR-based prediction. The correctness of this data is, in part, dependent on how effectively the operators recorded

and comprehended the linked experiments. In addition, the depth of the straight well's core sample is essential since only measurements taken at the level of the high-quality shale layer can correctly reflect the true properties of shale reservoirs. In addition, as indicated in Section 3.1, the average value of such a measurement is obtained after collecting four distinct types of core measurements from coring wells to reflect the unique reservoir attributes of each coring well. Due to the diversity of the shale or other geological factors, it is vital that the data quality of the average value precisely reflect the peculiarities of this coring well.

Similar to the input data, the output data was produced using statistical data from the comparable one-year shale gas production per stage for each horizontal well. The recordings produced by field operators have an effect on the data's quality. In addition, a number of operational factors, such as the shut-in, well testing, and other field operations, might influence this data [39]. Some quantitative and subjective factors restrict the overall quality of the employed data. In order to increase the data quality of this approach, future research would need include additional information.

5.2. Reservoir Properties

This research quantifies the effects of brittle mineral content, clay content, porosity, gas saturation, total organic carbon, production index, and brittleness index on shale productivity. Only data from thirteen wells were available for the area under examination, and the SGS method was used to estimate the spatial features of these properties. Additional information is required to properly appreciate these characteristics in future investigations and to define the reservoir parameters in their entirety. For example, reservoir characteristics might be obtained using the findings of a 3D seismic reflection interpretation, particularly in areas without well drilling [41–43]. Using the horizontal resolution of 3D seismic interpretation, the vertical resolution of logging interpretation, as well as core experiments [22], it is possible to more precisely define the reservoir's characteristics.

In this study, the SGS approach was used to generate a spatial picture of reservoir characteristics. We also compared it against a variety of interpolation methods, including the moving average, convergent interpolation, isochore interpolation, minimum curvature, and Kriging interpolation. Using the SGS method, the findings revealed a tight link between the regional features of shale output and the spatial distribution of reservoir properties.

In addition, the six input parameters (brittle mineral content, porosity, gas saturation, total organic carbon, production index, and brittleness index) were the parameters selected following the varied screening. Permeability, for instance, had a positive relationship with porosity; hence, it was not considered an input variable in the prediction model.

5.3. Data-Mining Methods

Recently, a range of machine-learning approaches has been used for data mining in order to determine the elements influencing shale production. These techniques often employ multiple linear regression, neural networks, and tree-based methods. Neural networks and tree-based techniques often require a large amount of training and testing data for improved prediction performance [38,43–47]. In this field scenario, such methodologies were unable to construct a substantially accurate model for estimating the shale gas production from a dataset of 130 wells. In this paper, we exclusively employed the MLR method. In future projects, we will include more data from new horizontal wells and experiment with sophisticated computational approaches to enhance the performance of our predictions.

Nonetheless, the MLR approach performs significantly better in terms of prediction when insufficient data is available [37]. On the basis of the findings of Section 4.2, it is possible to infer that the MLR-based prediction model is credible since the projected one-year shale gas output per stage nearly matches the actual output. Future studies will develop a huge number of datasets and investigate more machine-learning approaches to provide accurate predictions. In general, this paper's methodology may be used to direct the development of unconventional shale resources in various shale basins.

5.4. Regional-Level Assessment

The distinctive patterns of shale gas production in the studied region are shown in Figure 2, in which the production is influenced by many reservoir features. For the regional-level assessment of such a Duvernay shale resource near Fox Creek, previous researchers used geological or operational parameters to predict shale productivity in this region [48,49]. This work, however, conducted a comprehensive, multi-data analysis of reservoir characterization and proposed an integrated approach to reservoir characterization to evaluate the shale productivity of Duvernary shale. This work will lay the foundation for the future efficient development of shale gas resources in this region.

6. Conclusions

In this work, the gas output of the Duvernay shale play is determined through a comprehensive evaluation of many experimental data pertaining to reservoir properties. MLR is utilized to assess the relationship between annual output and reservoir parameters. Appropriate conclusions are drawn: (1) according to mineralogy data, the most abundant minerals in Duvernay shale are quartz, clay, and calcite; (2) the average values for effective porosity and permeability are 3.96% and 137.2 nD, respectively, whereas the average amount of total organic carbon (TOC) is 3.86%. The examined Duvernay shale was predominantly deposited in a gas-generating timeframe; (3) according to four triaxial compression investigations, the static Young's modulus ranges from 19.51 to 41.26 GPa, whereas the static Poisson's ratio ranges from 0.17 to 0.25; (4) the MLR method identifies the factors governing shale productivity, including PI, S_g, V_{cl}, F, TOC, BI, and BMC; and (5) the MLR-based prediction model accurately anticipates the output of shale gas. This research may be extended to other shale reservoirs to aid in the selection of optimal well locations, resulting in the effective exploitation of shale resources.

Author Contributions: G.H.: Conceptualization, Methodology, Software, Validation, Formal Analysis, Investigation, Resources, Data Curation, and Writing—Original Draft; F.G. and J.G.: Conceptualization, Methodology, Validation, Formal Analysis, and Editing; E.S.: Validation, Data Curation, Formal Analysis, Investigation. L.L.: Software, Formal Analysis, and Investigation. All authors have read and agreed to the published version of the manuscript.

Funding: This research was supported by Science Foundation of China University of Petroleum, Beijing (No. 2462023BJRC001).

Data Availability Statement: The well completion, well logs, core experiments, and production data used in this work were obtained from the geoSCOUT database (https://www.geologic.com/geoscout/ (accessed on 1 November 2022)).

Acknowledgments: We acknowledge the support from Hai Wang and Muming Wang at the University of Calgary.

Conflicts of Interest: The authors declare no conflict of interest.

Nomenclature

BI	brittleness index
BMC	brittle mineral content
ESB	Eastern Shale Basin
FESEM	field emission scanning electron microscope
HI	hydrogen index
MLR	multiple linear regression
OI	oxygen index
PI	production index

S1	adsorbed hydrocarbons
S2	kerogen pyrolysis
S_g	gas saturation
SGS	sequential Gaussian stochastic
T_{max}	maximum pyrolysis yield temperature
TOC	total organic carbon
V_{cl}	clay content
VR	vitrinite reflectance
WCSB	Western Canadian Sedimentary Basin
WSB	Western Shale Basin
Φ	effective porosity
a_i	an original independent variable at one site
a_{max}	maximum value among all "*a*" values
a_{min}	minimum value among all "*a*" values
n	number of parameters
x_i	*i*th standardized independent variable
Y	dependent variable
y_j	jth parameter after normalization
$\overline{y_j}$	mean value of predicted parameters
$\hat{y}_j$	predicted *j*th parameter
β_0	y-intercept
β_i	regression coefficient of the *i*th independent variables
ε	model error

References

1. Li, Q.; Chen, M.; Fred, P.W.; Jin, Y.; Li, Z. Influences of engineering factors on shale gas productivity: A case study from the Haynesville shale gas reservoir in North America. *Nat. Gas Ind.* **2012**, *32*, 54–59.
2. Wan, Y.; Li, Z.; Lu, B. The development of Fayetteville shale play and its implications. *Nat. Gas Geosci.* **2019**, *30*, 1655–1666.
3. Zou, C.; Pan, S.; Jing, Z.; Gao, J.; Yang, Z.; Wu, S.; Zhao, Q. Shale oil and gas revolution and its impact. *Acta Pet. Sin.* **2020**, *41*, 1–12.
4. IEA. *Natural Gas Information: Overview*; IEA: Paris, France, 2021; Available online: https://www.iea.org/reports/natural-gas-information-overview (accessed on 1 November 2022).
5. Zhao, W.; Xia, M.; Zhang, Y.; Zhang, F.; Zhang, Y.; Zhu, H. Current situation and progress of shale gas exploration and development in Canada. *Int. Pet. Econ.* **2013**, *21*, 41–46.
6. Dunn, L.; Schmidt, G.; Hammermaster, K.; Brown, M.; Bernard, R.; Wen, E.; Befus, R.; Gardiner, S. The Duvernay Formation (Devonian): Sedimentology and reservoir characterization of a shale gas/liquids play in Alberta. In Proceedings of the GeoConvention 2012: Vision, Calgary, AB, Canada, 14–18 May 2012.
7. Rokosh, C.D.; Lyster, S.; Anderson, S.D.A.; Beaton, A.P.; Berhane, H.; Brazzoni, T.; Chen, D.; Cheng, Y.; Mack, T.; Pana, C.; et al. *Summary of Alberta's Shale-and Siltstone-Hosted Hydrocarbon Resource Potential, Energy Resources Conservation Board*; ERCB/AGS Open File Report 2012-06; Energy Resources Conservation Board: Edmonton, AB, Canada, 2012; 327p.
8. Li, G.; Luo, K.; Shi, D. Key technologies, engineering management and important suggestions of shale oil/gas development: Case study of a Duvernay shale project in Western Canada Sedimentary Basin. *Pet. Explor. Dev.* **2020**, *47*, 739–749. [CrossRef]
9. Chen, S.; Zhu, Y.; Wang, H.; Liu, H.; Wei, W.; Fang, J. Shale gas reservoir characterization: A typical case in the southern Sichuan Basin of China. *Energy* **2011**, *36*, 6609–6616. [CrossRef]
10. Wang, W.; Zheng, D.; Sheng, G.; Zhang, Q.; Su, Y. A review of stimulated reservoir volume characterization for multiple fractured horizontal well in unconventional reservoirs. *Adv. Geo-Energy Res.* **2017**, *1*, 54–63. [CrossRef]
11. Wang, P.; Chen, Z.; Jin, Z. Optimizing Parameter "Total Organic Carbon Content" for Shale Oil and Gas Resource Assessment: Taking West Canada Sedimentary Basin Devonian Duvernay Shale as an Example. *Earth Sci.* **2018**, *44*, 504–512.
12. Song, X.; Zhang, C.; Shi, Y.; Li, G. Production performance of oil shale in-situ conversion with multilateral wells. *Energy* **2019**, *189*, 116145. [CrossRef]
13. Nie, H.; Tang, X.; Bian, R. Controlling factors for shale gas accumulation and prediction of potential development area in shale gas reservoir of South China. *Acta Pet. Sin.* **2009**, *30*, 484–491.
14. Liao, D. Evaluation Methods and Engineering Application of the Feasibility of "Double Sweet Spots" in Shale Gas Reservoirs. *Pet. Drill. Tech.* **2020**, *48*, 94–99.
15. Ma, W.; Li, Z.; Sun, Y.; Zhang, J.P.; Deng, S.Z. Non-Deterministic Shale Gas Productivity Forecast Based on Machine Learning. *Spec. Oil Gas Reserv.* **2019**, *26*, 101–105.
16. Jing, G.; Chen, Z.; Hu, X.; Hui, G. Influence of different shut-in periods after fracturing on productivity of MFHW in Duvernay shale gas formation with high montmorillonite content. *Fuel* **2021**, *314*, 122719. [CrossRef]
17. Kong, B.; Chen, S.; Chen, Z.; Zhou, Q. Bayesian probabilistic dual-flow-regime decline curve analysis for complex production profile evaluation. *J. Pet. Sci. Eng.* **2020**, *195*, 107623. [CrossRef]

18. Yasin, Q.; Sohail, G.M.; Liu, K.Y.; Du, Q.Z.; Boateng, C.D. Study on brittleness templates for shale gas reservoirs—A case study of Longmaxi shale in Sichuan Basin, southern China. *Pet. Sci.* **2021**, *18*, 1370–1389. [CrossRef]
19. Jiang, R.; Zhao, L.; Xu, A.; Ashraf, U.; Yin, J.; Song, H.; Su, N.; Du, B.; Anees, A. Sweet spots prediction through fracture genesis using multi-scale geological and geophysical data in the karst reservoirs of Cambrian Longwangmiao Carbonate Formation, Moxi-Gaoshiti area in Sichuan Basin, South China. *J. Pet. Explor. Prod. Technol.* **2022**, *12*, 1313–1328. [CrossRef]
20. He, X.; Gao, Y.; Tang, X.; Zhang, P.; He, G. Analysis of major factors controlling the accumulation in normal pressure shale gas in the southeast of Chongqing. *Nat. Gas Geosci.* **2017**, *28*, 654–664.
21. Hui, G.; Chen, S.; He, Y. Production forecast for shale gas in unconventional reservoirs via machine learning approach: Case study in Fox Creek, Alberta. *J. Nat. Gas Sci. Eng.* **2021**, *94*, 104045. [CrossRef]
22. Kong, X.; Wang, P.; Xia, Z. Geological characteristics and fluid distribution of the Upper Devonian Duvernay shale in Simonette block in the Wester Canada Sedimentary Basin. *China Pet. Explor.* **2022**, *27*, 93–107.
23. Jiang, R.; Ji, Z.; Mo, W.; Wang, S.; Zhang, M.; Yin, W.; Wang, Z.; Lin, Y.; Wang, X.; Ashraf, U. A Novel Method of Deep Learning for Shear Velocity Prediction in a Tight Sandstone Reservoir. *Energies* **2022**, *15*, 7016. [CrossRef]
24. Ashraf, U.; Zhang, H.; Anees, A.; Mangi, H.N.; Ali, M.; Zhang, X.; Imraz, M.; Abbasi, S.S.; Abbas, A.; Ullah, Z.; et al. A Core Logging, Machine Learning and Geostatistical Modeling Interactive Approach for Subsurface Imaging of Lenticular Geobodies in a Clastic Depositional System, SE Pakistan. *Nat. Resour. Res.* **2021**, *30*, 2807–2830. [CrossRef]
25. Switzer, S.B.; Holland, W.G.; Christie, D.S.; Graf, G.C.; Hedinger, A.S.; McAuley, R.J.; Wierzbicki, R.A.; Packard, J.J.; Mossop, G.D.; Shetsen, I. DevonianWoodbend-Winterburn Strata of the Western Canada Sedimentary Basin. In *Geological Atlas of the Western Canada Sedimentary Basin*; Mossop, G., Shetsen, I., Eds.; Canadian Society of Petroleum Geologists and Alberta Research Council: Calgary, AB, Canada, 1994.
26. Shen, L.W.; Schmitt, D.R.; Wang, R.; Hauck, T.E. States of in situ stress in the Duvernay East Shale Basin and Willesden Green of Alberta, Canada: Variable in situ stress states effect fault stability. *J. Geophys. Res. Solid Earth* **2021**, *126*, e2020JB021221. [CrossRef]
27. Price, R.N. Cordilleran tectonics and the evolution of the western Canada sedimentary basin. In *Geologic Atlas of the Western Canada Sedimentary Basin*; Mossop, G.D., Shetsen, I., Eds.; Canadian Society of Petroleum Geologists and Alberta Research Council: Calgary, AB, Canada, 1994; pp. 13–24.
28. Lyster, S.; Corlett, H.J.; Berhane, H. *Hydrocarbon Resource Potential of the Duvernay Formation in Alberta—Update*; AER/AGS Open-file Report 2017-02; Energy Resources Conservation Board: Edmonton, AB, Canada, 2017; 44p.
29. Hui, G.; Gu, F.; Chen, Z. Integration of Mineralogy, Petrophysics, Geochemistry and Geomechanics to Evaluate Unconventional Shale Resources. In Proceedings of the SPE Asia Pacific Oil & Gas Conference and Exhibition, Adelaide, Australia, 17–19 October 2022.
30. Hui, G.; Chen, S.; Chen, Z.; He, Y.; Wang, S.; Gu, F. Investigation on Two Mw 3.6 and Mw 4.1 Earthquakes Triggered by Poroelastic Effects of Hydraulic Fracturing Operations near Crooked Lake, Alberta. *J. Geophys. Res. Solid Earth* **2021**, *126*, e2020JB020308. [CrossRef]
31. Zhang, Q.; Littke, R.; Zieger, L.; Shabani, M.; Tang, X.; Zhang, J. Ediacaran, Cambrian, Ordovician, Silurian and Permian shales of the Upper Yangtze Platform, South China: Deposition, thermal maturity and shale gas potential. *Int. J. Coal Geol.* **2019**, *216*, 103281. [CrossRef]
32. Zoback, M. *Reservoir Geomechanics*; Cambridge University Press: Cambridge, UK, 2007.
33. Hui, G.; Chen, S.; Chen, Z.; Jing, G.; Hu, D.; Gu, F. Role of Fluid Diffusivity in the Spatiotemporal Migration of Induced Earthquakes during Hydraulic Fracturing in Unconventional Reservoirs. *Energy Fuels* **2021**, *35*, 17685–17697. [CrossRef]
34. Pan, X.; Zhang, G.; Chen, J. The construction of shale rock physics model and brittleness prediction for high-porosity shale gas-bearing reservoir. *Pet. Sci.* **2020**, *17*, 658–670. [CrossRef]
35. Hui, G.; Chen, Z.; Chen, S.; Gu, F. Hydraulic fracturing-induced seismicity characterization through coupled modeling of stress and fracture-fault systems. *Adv. Geo-Energy Res.* **2022**, *6*, 269–270. [CrossRef]
36. Hui, G.; Chen, S.; Chen, Z.; Gu, F.; Ghoroori, M.; Mirza, M.A. Comprehensive characterization and mitigation of hydraulic fracturing-induced seismicity in Fox Creek, Alberta. *SPE J.* **2021**, *26*, 2736–2747. [CrossRef]
37. Pawley, S.; Schultz, R.; Playter, T.; Corlett, H.; Shipman, T.; Lyster, S.; Hauck, T. The geological susceptibility of induced earthquakes in the Duvernay play. *Geophys. Res. Lett.* **2018**, *45*, 1786–1793. [CrossRef]
38. Hui, G.; Chen, Z.; Wang, Y.; Zhang, D.; Gu, F. An integrated machine learning-based approach to identifying controlling factors of unconventional shale productivity. *Energy* **2023**, *266*, 126512. [CrossRef]
39. Hui, G.; Chen, S.; Chen, Z.; Gu, F. An integrated approach to characterize hydraulic fracturing-induced seismicity in shale reservoirs. *J. Pet. Sci. Eng.* **2021**, *196*, 107624. [CrossRef]
40. Yew, C.H.; Wei, X. *Mechanics of Hydraulic Fracturing*, 2nd ed.; Gulf Professional Publishing: Oxford, UK, 2015.
41. Hui, G.; Chen, S.; Gu, F.; Wang, H.; Zhang, L.; Yu, X. Influence of hydrological communication between basement-rooted faults and hydraulic fractures on induced seismicity: A case study. *J. Pet. Sci. Eng.* **2021**, *206*, 109040. [CrossRef]
42. Hui, G.; Chen, Z.; Wang, P.; Gu, F.; Kong, X.; Zhang, W. Mitigating risks from hydraulic fracturing-induced seismicity in unconventional reservoirs: Case study. *Sci. Rep.* **2022**, *12*, 12537. [CrossRef]
43. Hui, G.; Chen, Z.X.; Lei, Z.D.; Song, Z.J.; Zhang, L.Y.; Yu, X.R.; Gu, F. A synthetical geoengineering approach to evaluate the largest hydraulic fracturing-induced earthquake in the East Shale Basin, Alberta. *Pet. Sci.* 2023, *in press*. [CrossRef]
44. Shelley, B.; Stephenson, S. The use of artificial neural networks in completion stimulation and design. *Comput. Geosci.* **2000**, *26*, 941–951. [CrossRef]
45. Hui, G.; Gu, F. An integrated method to mitigate hazards from hydraulic fracturing–induced earthquakes in the Duvernay Shale Play. *SPE Reserv. Eval. Eng.* 2022, *in press*. [CrossRef]

46. Awoleke, O.O.; Lane, R.H. Analysis of data from the Barnett shale using conventional statistical and virtual intelligence techniques. *SPE Reserv. Eval. Eng.* **2022**, *14*, 544–556. [CrossRef]
47. LeCun, Y.; Bengio, Y.; Hinton, G. Deep learning. *Nature* **2015**, *521*, 436–444. [CrossRef] [PubMed]
48. Wang, S.; Chen, S. Insights to fracture stimulation design in unconventional reservoirs based on machine learning modeling. *J. Pet. Sci. Eng.* **2019**, *174*, 682–695. [CrossRef]
49. Wang, H.; Chen, Z.; Chen, S.; Hui, G.; Kong, B. Production forecast and optimization for parent-child well pattern in unconventional reservoirs. *J. Pet. Sci. Eng.* **2021**, *203*, 108899. [CrossRef]